Sustainable Energy Technologies and Assessments 56 (2023) 103006

Contents lists available at ScienceDirect

Sustainable Energy Technologies and Assessments

journal homepage: www.elsevier.com/locate/seta

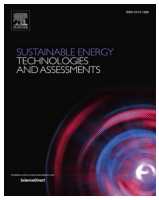

MOF based coated adsorption system for water desalination and cooling integrated with Pre-treatment unit

Ibrahim Albaik [a,*], Kamal E. Diab [a], Majdi Saleh [a], Raya Al-Dadah [a], Saad Mahmoud [a], Mahmoud B. Elsheniti [b,c], İsmail Solmaz [d,e], Eslam Salama [f], H. Shokry Hassan [g,h], Marwa F. Elkadi [i,j]

[a] Department of Mechanical Engineering, University of Birmingham, Edgbaston, Birmingham B15 2TT, UK
[b] Mechanical Engineering Department, College of Engineering, King Saud University, Riyadh 11451, Saudi Arabia
[c] Mechanical Engineering Department, Faculty of Engineering, Alexandria University, El-Chatby, Alexandria 21544, Egypt
[d] Department of Mechanical Engineering, Ataturk University, 25240 Erzurum, Turkey
[e] RENTECH Renewable Energy Technologies LLC Atatürk University Campus, Technology Development Zone, Yakutiye/Erzurum/Turkey
[f] Environment and Natural Materials Research Institute (ENMRI), City of Scientific Research and Technological Applications (SRTA City), New Borg El Arab City, Alexandria 21934, Egypt
[g] Environmental Engineering Department, Egypt Japan University of Science and Technology, New Borg El Arab City, Alexandria 21934, Egypt
[h] Electronic Materials Researches Department, Advanced Technology and New Materials Researches Institute, City of Scientific Researches and Technological Applications (SRTA City), New Borg El Arab City, Alexandria 21934, Egypt
[i] Chemical and Petrochemical Engineering Department, Egypt Japan University of Science and Technology (E JUST), New Borg El Arab City, Alexandria 21934, Egypt
[j] Fabrication Technology Research Department, Advanced Technology and New Materials Research Institute, City of Scientific Research and Technological Applications (SRTA City), New Borg El Arab City, Alexandria 21934, Egypt

A B S T R A C T

Recently, the adsorption technologies received significant interest for water purification and desalination application as well as for clean cooling production, since they offer an environmentally friendly solution using low-grade energy compared to the conventional systems. In this work, a hybrid adsorption system based on combining a pre-treatment unit for heavy metal removal with a desalination and cooling unit is experimentally investigated. Activated carbon and zeolite in powder and beads forms have been used in pre-treatment unit as adsorbent materials for the removal of iron, lead, manganese and nickel from ground water, while a coating form of aluminium fumarate MOF adsorbent material is used in heat powered adsorption heat pump for desalination and cooling unit. For the formation of activated carbon/zeolite beads, 45 % polymer loading showed the highest efficiency for the removal of the heavy metals which reached 87 % of iron. After taking the purified water from the pretreatment unit, the desalination and cooling unit produced higher than 260L/day of distilled water and 6.9 kW of cooling power with a coefficient of performance of 0.26 using a coating thickness of 0.75 mm on the wire finned tube heat exchanger adsorber beds. With the hybrid system, a practical mitigation of the accumulation of some chemical compounds on the evaporator surface with continuous operation was achieved. The effect of evaporator and condenser chamber volumes are investigated to minimize the compactness of the MOF adsorption heat pump. This hybrid adsorption system demonstrates a promising solution for pure water and cooling production over the conventional available ones.

Introduction

With the population growth worldwide, the freshwater demands are increasing dramatically, while the water resources cannot be utilized directly due to two main factors. Firstly, agriculture and industrial processes have contaminated freshwater sources with numerous inorganic and organic pollutants [1,2] and secondly, most groundwater used for drinking and irrigation contains various ions and salts [1].

Regarding the inorganic and organic contaminants, finding ways to effectively alleviate this pollution is of paramount importance to protect and improve human, animal and aquatic life, and environment [3]. Heavy metals such as iron, nickel, manganese and lead are commonly occurring the most inorganic contaminants in water supplies [4–6]. It was found that heavy metals have harmful impacts on human life and health which may lead to nervous system diseases, respiratory paralysis and brain cancer [7] Moreover, heavy metals poisoning causes symptoms such as headaches, dizziness, tearing nausea, memory problems and blurred vision [8] However, the sources of heavy metals in agriculture are still ongoing in many countries all over the world [5,9,10]. Many strategies have been investigated for the removal of contaminants

* Corresponding author.
E-mail address: i.albaik1993@gmail.com (I. Albaik).

https://doi.org/10.1016/j.seta.2022.103006
Received 6 June 2022; Received in revised form 3 November 2022; Accepted 30 December 2022
Available online 20 January 2023

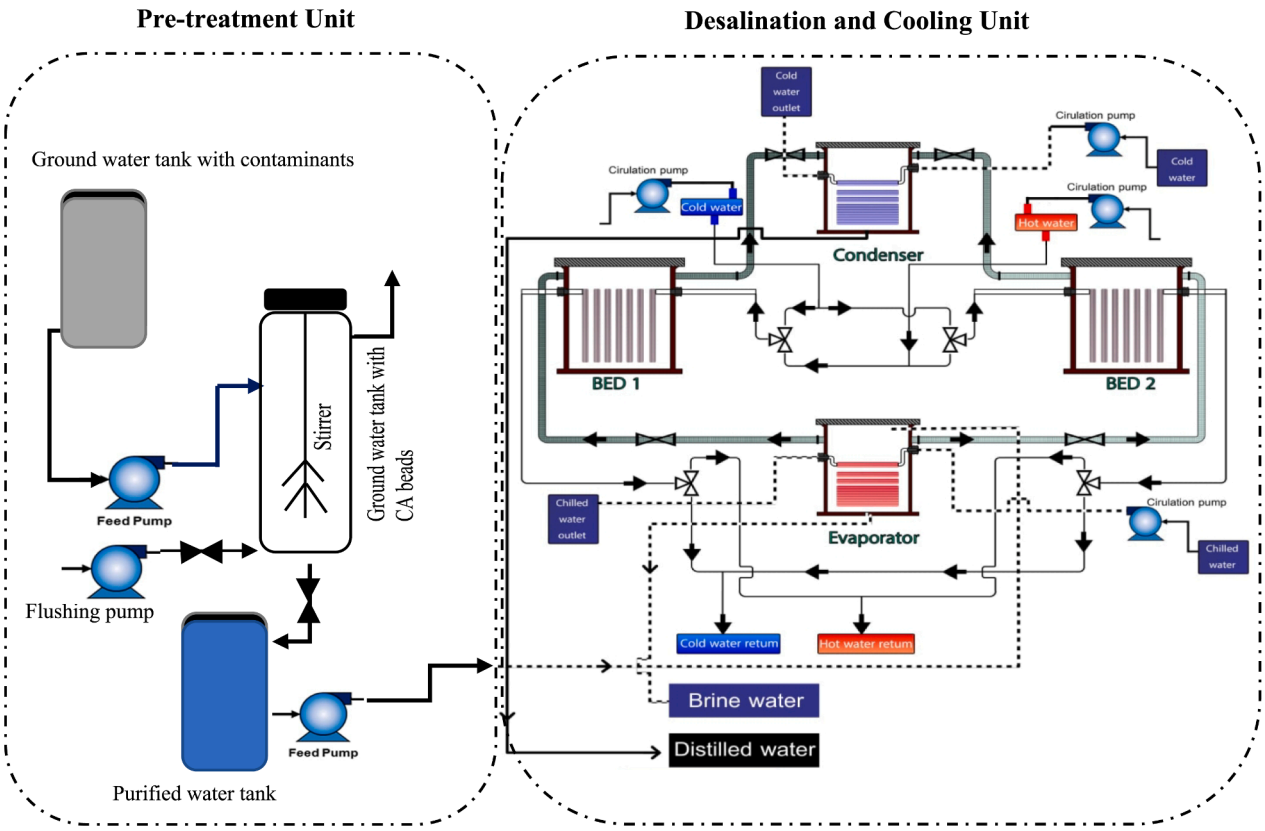

Fig. 1. Schematic diagram of the adsorption based waste water treatment system.

from water including coagulation [11] chemical and biological oxidation, photocatalytic degradation and ozonation [12]. However, these methods have one or more of the following drawbacks such as inefficient or moderate removal capacity, high operational energy costs, formation of toxic oxidation by products and production of large quantity of sludge [7] Alternatively, adsorption is an effective, relatively inexpensive, and harmless method that showed promising results in resolving heavy metals removal [11,13] Specifically, activated carbon and zeolite materials have been examined as sorbents for pollutants removal [14,15] However, the low adsorption capacity of the activated carbon for organic and inorganic contaminants and the difficulty of its regeneration remain challenging issues to be resolved [16].

Regarding the salt content in water, the desalination systems are becoming essential to deliver freshwater for agriculture, industrial and household applications. Three main desalination technologies are widely used which are: Reverse Osmosis (RO), multistage flash (MSF) and multi effect distillation (MED) [17]. These technologies suffer from high energy consumption, CO_2 emissions and water production cost [18]. Recently, adsorption desalination systems using new metal organic framework (MOF) adsorbent materials which have high water uptake and surface area compared to the conventional adsorbent materials like silica gel, zeolite and activated carbon (which has only a surface area between 150 m2/g to 3100 m2/g [19]), have been developed to deliver cheaper water production with environmentally friendly solution. These systems are basically operated by evaporating the water from the saline water at the evaporator during the adsorption process, then the adsorbent water vapor will be regenerated and condensed in the condenser to be collected as a fresh water. Additionally, a cooling effect can also be produced during the adsorption process, which is considered as an extra production during the freshwater production. Recently, aluminium fumarate, CPO-27 Ni and MIL-101 Cr are some MOFs that used for this purpose [20–22]. However, applying the MOF material into the heat exchanger of the adsorber bed to get the highest system performance is a big challenge that need to be investigated in order to deliver a good heat and mass transfers to the material. Also, further studies need to be carried on to optimize the specific water daily production (SDWP) and specific cooling power (SCP) to get the highest water production from minimum adsorbent material.

Therefore, combining the same technology (adsorption) to remove organic & inorganic contaminants and desalinate the salty water in a hybrid adsorption system will be a unique solution to deliver freshwater by using effective adsorbent material candidates (activated carbon and MOF) for contaminants removal and desalination. Additionally, despite of using the stainless-steel coils in the evaporator of the desalination and cooling unit, this material might have corrosion when it exposed to heavy metals like iron and nickel due to the formation of different chemical compounds such as iron carbides and nitrides [23]. Thus, removing the heavy metals by a pre-treatment unit before passing the water to the desalination and cooling unit is essential.

Recently, production of highly porous activated carbon with large surface area from agricultural wastes has been investigated using environment friendly methods for example using a water hyacinth plant, one of the agricultural waste plants as a precursor for activated carbon production contribute to the environmental protection issue. Accordingly, the production of nano-magnetic activated carbon (NMAC) from water hyacinth has potential economic and environmental impacts. First, it converts unwanted, low-value aquatic plants to useful and high-value sorbents. Second, the production of NMAC represents novel adsorbent material for water purification. Furthermore, since activated carbon sufferers from low volumetric capacity, the use of excessive amount of sorbents is necessary which results in a moderately expensive strategy [24,25] Therefore, a recyclable, cost-effective and high capacity materials to remove heavy metals from water must be designed to ensure efficient decontamination of water. Also, it is still challenging to prepare activated carbon composites that offer high surface area and performance similar to the parent materials using green strategies to get an

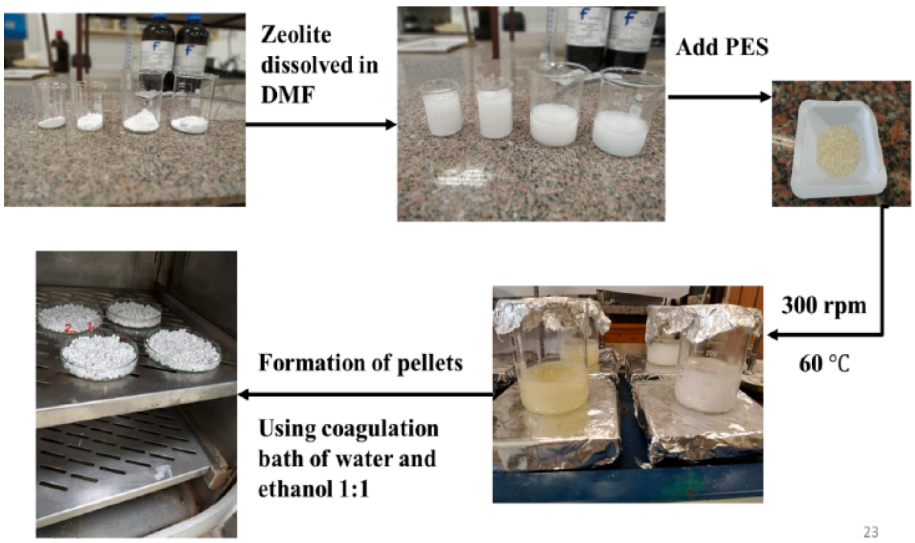

Fig. 2. Procedures of fabrication Zeolite/PES composite beads using phase inversion technique.

industrial applicable form of sorbent powder [26,27].

On the other hand, most adsorption desalination systems are suffering from low thermal conductivity and high contact thermal resistance with metal surfaces when granular adsorbent materials are packed in the adsorber bed heat exchangers [28]. Coating the surfaces with the adsorbent material by mixing the material powder with a binder agent is used as an alternative solution to increase the heat transfer and reduce the contact thermal resistance [29,30]. However, increasing the coating thickness may lower with the mass transfer as the binding agent can block the voids through the adsorbent material, while reducing the coating thickness results in increasing the metal to adsorbent mass ratio leading to higher energy consumption. Therefore, further studies need to be carried out to optimize the coating thickness without having a significant impact on the mass transfer.

In this paper, a combination between the activated carbon and coated MOF in the adsorption system to deliver a fresh water by removing organic/inorganic contaminants and salts from water will be studied experimentally. The authors report here a facile and scalable strategy for the fabrication of millimetre-sized activated carbon composite beads that are constructed from chitosan and sodium alginate in form of biocompatible beads, named chitosan-alginate beads (CA). The CA beads are used in a treatment unit to decontaminate organic and inorganic pollutants from wastewater. The pre-treated waste water is then applied to a MOF coated adsorption system with coating thickness higher than thicknesses reported in the literature (0.75 mm) in order to deliver high SDWP in the desalination system.

Hybrid system description

The hybrid system consists mainly of two units; the pre-treatment unit and the desalination and cooling unit in which both units are connected in series as shown in Fig. 1. In the pre-treatment unit, a specific amount of feed solution of ground water with contaminants (Fe, Pb, Mn and Ni) is fed to the activated carbon/zeolite beads tank. The contaminated water is then purified in the CA tank over 2–3 h with all the valves switched off and the stirrer is operated. The valve in the bottom of the tank is then switched on in order to collect the purified water in the purified water tank. Before starting a new cycle in the pre-treatment unit, a flushing pump will regenerate the material by feeding water in the opposite direction of the original flow. After a number of cycles, the purified water tank is fed to the evaporator of the MOF adsorption desalination and cooling unit. During the adsorption phase in the first bed, chilled water is fed to the evaporator as well as cooling water is fed to the first bed in which the adsorbent material (MOF) is coated onto the heat exchanger surfaces inside the bed. Pure water vapor will pass from the evaporator to the first bed due to the affinity of the MOF adsorbent material to water vapor which causes further water evaporation in the evaporator and production of cooling. On the other hand, the second bed will be working in the desorption phase in which the adsorbent material in the bed is regenerated by feeding hot water to the heat exchangers, while the desorbed vapour is collected in the condenser in which cooling water is fed to the condenser. Once the adsorption and desorption phases are completed in the first and second beds respectively, the beds will swich the phases between each other to ensure having a continuous fresh water production (distilled water) that can be collected from the condenser as well as a continuous cooling production from the evaporator. By this approach, the hybrid system can purify the water from heavy metals contaminates using activated carbon/zeolite as a first stage followed by a water desalination and cooling production using aluminium fumarate as a second phase. These contaminants would have a negative impact on the evaporation process and heat exchanger metals if the pre-treatment unit is not integrated with the desalination and cooling system [23].

Methodology

In this work, the hybrid system contains two adsorbent materials, where activated carbon and zeolite are used in the pre-treatment unit for the removal of heavy metals, while aluminium fumarate MOF material is used in the heat powered adsorption desalination and cooling unit using the coating approach. In this section, the preparation and synthesis procedures for these materials are described, followed by characterizing the materials using powder X-ray diffraction (PXRD), Fourier *T*-infra red (FTIR), scanning electron microscope (SEM) and dynamic vapor sorption apparatus (DVS). Adsorption pre-treatment unit and desalination and cooling unit experiment procedures are also described.

Preparation of sorbent materials for Pre-treatment unit

Both extracted nano-activated carbon from the water hyacinth roots and synthetized zeolite from clay were investigated for the adsorption of heavy metals commonly existing in manganese, iron, lead and nickel ions. Since the recovery of powder adsorbent materials after water treatment process is difficult, and their operation in powder form in wastewater treatment process cause a high-pressure drop under column operation, the powders will be immobilized in different weight ratios

Fig. 3. Aluminum fumarate preparation for coating (a) distilled water mixed with binder (b) mixing distilled water and binder with adsorbent material powder.

onto poly ether sulfones (PES) polymeric matrix to be formulated into bead-shaped composite adsorbent materials. The adsorption performance of the different formulated beads with different weight ratio for both synthetized materials was determined toward the most selective predetermined contaminated metal ion using batch technique. The optimum immobilized weight ratio from both nano-activated carbon and zeolite were determined. The optimum fabricated composite beads from both zeolite-PES and nano-activated carbon-PES were characterized using different physico-chemical technique including SEM, FTIR and XRD.

The composite beads were fabricated using phase inversion technique where a specific amount from nano-activated carbon powder or zeolite was dispersed into 10 ml from DMF solvent by mechanical stirring for 24 h under heating at 60 °C as shown in Fig. 2. Then, 1 g from the PES polymeric powder was added gradually to the solution while stirring. The nano-activated carbon-PES (NAC/PES) and zeolite polymeric solution was stirred for 24 h at 60 °C to complete dissolution of the polymer and successful dispersion of nano-activated or zeolite powder into the polymeric matrix. In order to formulate this solution into beads using phase inversion technique, this composite solution was added dropwise to cold coagulation bath at 10 °C included 10 ml ethanol and 10 ml distilled water and maintained stirring for 5 min to ensure complete polymer precipitation and separation of the solvent from polymeric composite matrix to form NAC/PES and zeolite/PES composite beads. In order to complete the separation of DMF solvent from the composite beads to form pores at the beads, the formulated beads collected from cold coagulation bath was refreshed through soaking in ethanol solution. Then the solvent free NAC/PES and zeolite/PES composite beads were dried at 35 °C. Additionally, all the prepared composite beads were activated before their utilization at the water treatment process by heating at 140 °C for an hour under vacuum to remove any solvent molecules from their pores as indicated at Fig. 2. Four different NAC/PES and zeolite/PES composite beads were fabricated through varying the immobilized percentages of nano-activated carbon and zeolite filler (25, 45, 65 and 85 wt%) at the polyether sulfones (PES) solution. 45 wt% of NAC/PES and zeolite/PES composite beads showed an excellent stability and shape reservation in comparison to other loading percentages.

Characterization of sorbent materials for Pre-treatment unit

As shown in Figure X1(a), it was evident from XRD pattern of the optimum fabricated NAC/PES 45 % composite beads that the structure of the activated carbon is well maintained during the synthesis process (Figure X1(a)). A close inspection of PXRD revealed that the activated carbon is interacting well with the polymeric material while maintaining the amorphous structure of activated carbon stable under the conditions of formation of the composite beads. The polymeric PES is primarily amorphous material and it has characteristics only of small peak at $2\theta = 18.2^{\circ}$, while, NAC is characterized by its broad diffraction peak at $2\theta = 15\text{-}30^{\circ}$ that confirms its amorphous carbon structures. The weak and broad diffraction peak at $2\theta = 40\text{-}50^{\circ}$ is due to the a-axis of the graphite structure at the immobilized NAC matrix. So, due to the amorphous structure of both nano-activated carbon and PES, no characteristic peak was identified for the prepared NAC/PES 45 % composite beads as shown from the PXRD. However, the PXRD revealed a good compatibility between the activated carbon and polyether sulphone polymeric matrices. As shown Figure X1(b), FTIR spectra of prepared NAC/PES 45 % composite beads was carried out to confirm the embedment of nano-activated carbon material at the poyymeric matrix. Where, the spectra showed the characteristics PES peaks, the peaks at 1244 and 1141 cm^{-1} are supposed to be the stretching vibrations of S═O asymmetric and S═O symmetric of PES, which correlates well with the previously reported literature [31]. The peak of O—H stretching vibration at about 3400–3600 cm^{-1} and C═O bonds at 1660 cm^{-1} are corresponding to NAC. Accordingly, the FTIR spectra confirming that the combination between NAC and PES at the prepared NAC/PES 45 % composite beads. As shown Figure X1(c) SEM images reveal that the prepared NAC/PES 45 % composite beads with the amorphous activated carbon have a porous morphology with a size of 3.5 ± 0.7 mm. A high magnification of SEM shows a good interaction of activated carbon with PES while maintaining the activated carbon exposed for adsorption of pollutants as shown in Figure X1(c). Also, the SEM images confirm the suitable dispersion of NAC nanoparticles in the polymeric beads matrix. This uniform distribution of the nanoparticles is favourable because it increases the contact area of the passing polluted water through the beads and the surface of the particles, which subsequently increases the surface adsorption of the metal ions from contaminated water.

PXRD of zeolite beads suggested that the crystal structure of the zeolite is well maintained during the structuring process of formulated zeolite/PES 45 % composite beads (Figure X2(a)). A close inspection of PXRD revealed that the zeolite is interacting well with the polymeric PES matrix while maintaining the structure of zeolite stable under the conditions of formation of the composite beads. Where, as evident from Figure X2(a), all the characteristics sharp peaks of zeolite were identified. Less peak shift was apparent between the prepared pristine zeolite investigated and the composite zeolite beads, meaning that the

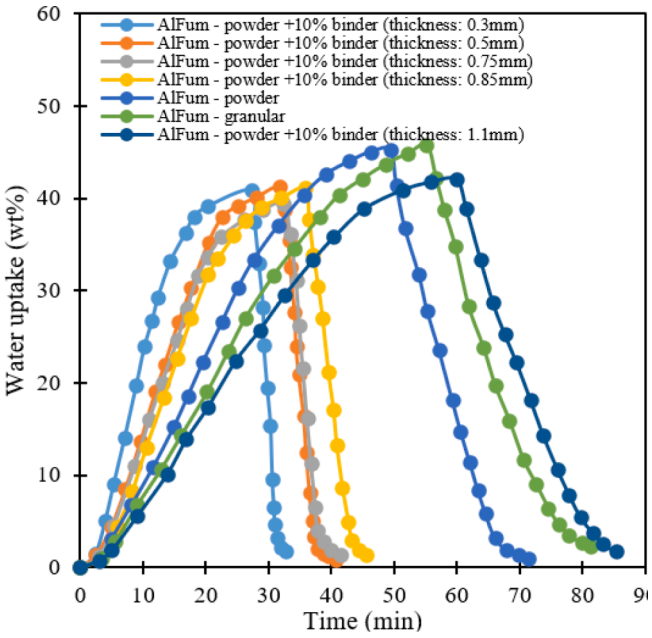

Fig. 4. Water cyclic performance at different coating thicknesses.

crystalline structure of the zeolite caused no change in the 45 % zeolite/PES composite beads. FTIR spectra of prepared 45 % zeolite/PES composite beads were carried out to confirm the interaction between prepared zeolite material and polymeric PES matrix at the polymeric composite matrix (Figure X2(b)). Where, the spectra showed the characteristics PES peaks, the peaks at 1244 and 1141 cm^{-1} are supposed to be the stretching vibrations of S═O asymmetric and S═O symmetric of PES, which correlates well with the previously reported literature [27]. The peak at 1050 cm^{-1} and 765 cm^{-1}, were related to the Si-O-Si and Si-O symmetric and asymmetric vibrations respectively in the zeolite matrix. Meanwhile, the shoulder peaks at 1200 cm^{-1} and 700 cm^{-1} could be attributed to the Al-OH and Si-O bending vibration respectively which are corresponding to zeolite. Accordingly, the FTIR spectra confirms the combination between zeolite and PES at the prepared zeolite/PES 45 % composite beads. SEM images reveal that the synthesized composite polymeric beads with the crystallites zeolite have a porous morphology with a size of 4.6 ± 0.8 mm. A high magnification of SEM shows a good interaction of zeolite particles with PES as shown in Figure X2(c). As the prepared zeolite powder is well distributed in the PES network with a sponge structure as evident from high resolution SEM images.

Preparation MOF adsorbent material for the adsorption heat pump desalination and cooling unit

Fig. 3 shows the preparation of aluminium fumarate MOF adsorbent material (purchased from MOF Technology Co. in a powder form) for coating. 2000 ml of distilled water is heated and mixed with 40 g of binder agent (hydroxy ethyl cellulose) at temperature of 90 °C for 30 min, followed by mixing 400 g of aluminium fumarate powder with the solution for another 30 min under stirring.

Characterization of MOF adsorbent material for adsorption heat pump desalination and cooling unit

To examine the effect of coating thickness performance in adsorption heat pump for cooling and desalination applications, five different coating thicknesses (0.3, 0.5, 0.75, 0.85 and 1.1 mm) were prepared in order to be tested using dynamic vapour sorption apparatus (DVS). A cyclic performance study was conducted using an adsorption temperature of 25 °C and desorption temperature of 90 °C at a relative pressure of 90 % in the adsorption process as shown in Fig. 4. The fastest kinetic was observed using the coating thickness of 0.3 and 0.5 mm in which the cycle time were only 35 and 45 min respectively. This kinetic is much faster than using the conventional packing method of adsorbent granular which showed a cycle time of 85 min due to the higher thermal conductivity and lower contact resistance that caused by using the binder. In terms of the gravimetric water uptake, the coating method using 0.3 mm can provide double the SCP and SDWP values compared to the packing one. However, due to the thin coating thickness, the coating method requires more heat exchanger surfaces which ultimately increases the required heat exchanger mass that needs more energy to heat up the adsorbent material in the regeneration process which illustrated in details in comparison study between the packing and coating methods [32]. Therefore, in this study more investigations were performed at thicker layers such as 0.75, 0.85 and 1.1 mm. It is reported that the cycle time did not significantly increase at coating thickness of 0.75 mm compared to 0.5 mm. In 1.1 mm coating thickness, the cycle time exceeded the packing method due to the impact of binder in blocking the pores of the adsorbent material. These results showed that there is an opportunity to decrease the heat exchanger mass by using thicker coating layer compared to Elsayed et al. [33] who investigated thicknesses up to only 0.5 mm, which ultimately can increase the COP of the adsorption system since less heating energy will be required in the regeneration process.

Coating the heat exchanger for adsorber beds

Fig. 5 shows the wire finned tube heat exchanger module coated with

Fig. 5. (a) Adsorbent material spraying and (b) initial drying before placing the heat exchanger in the oven.

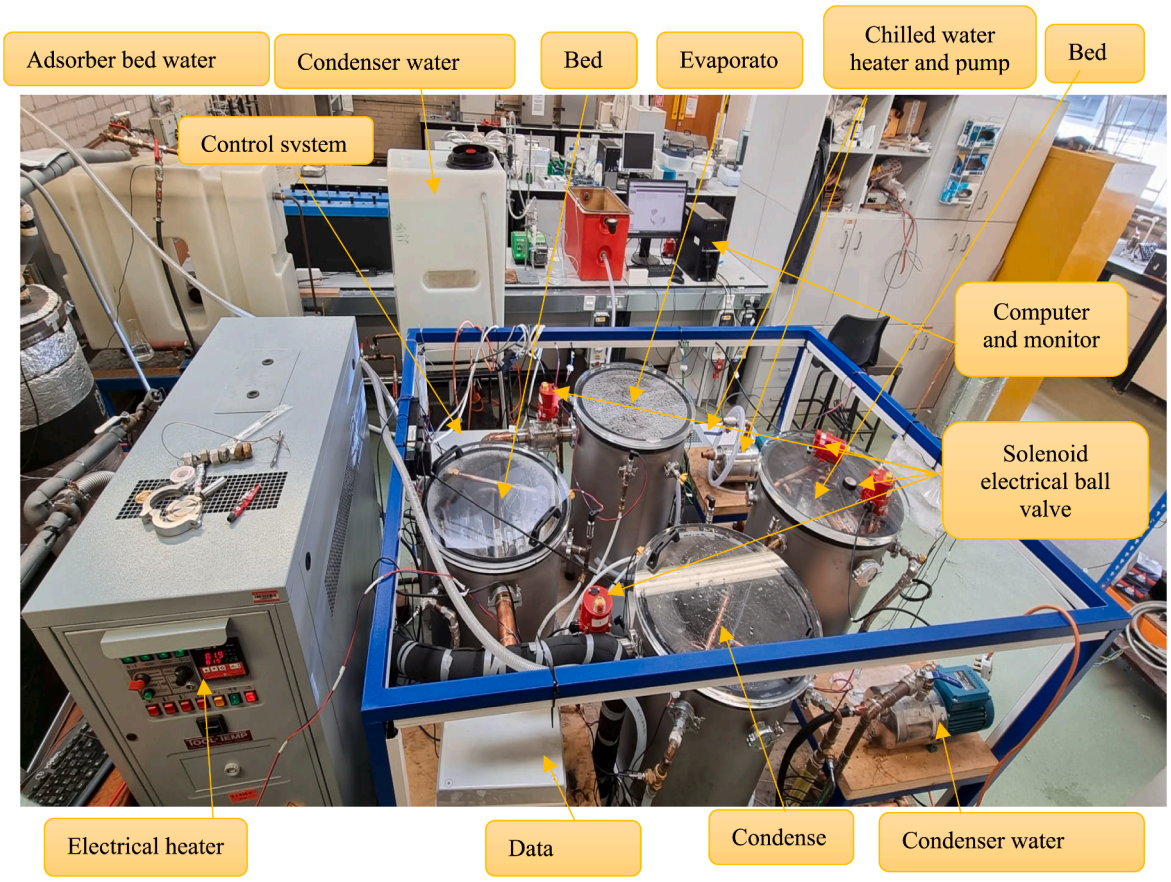

Fig. 6. Two-bed adsorption heat pump system for desalination and cooling.

0.75 mm of adsorbent material thickness, where several layers of coating the adsorbent material were applied in order to obtain this thickness. The first layer of adsorbent material is sprayed on the heat exchanger surface until achieving 0.1 mm coating thickness. Then an electrical heater gun is used for drying the adsorbent material for 5 min in order to dry it to avoid dripping of adsorbent material when the module is placed inside the oven. Then, the module is placed in the oven at 90 °C for 120 min in order to ensure having a solid layer of coated material before starting the next coating layer. The coating procedure is repeated until achieving the required thickness. The intermediate coating layers are placed in the oven for only 60 min. The last coating layer needs to stay in the oven over night at 70 °C to ensure having a fully dried adsorbent material. Finally, the coating thickness is measured using two methods. The first one is by using a digital calliper with a tolerance of 0.01 mm, so that the coating thickness is equal to $(\frac{themeasuredoverallmetalwirewiththecoatedlayerthicknesses}{wiremetalthickness(1mm)*2})$. The second one is by weighing the heat exchanger module before and after the coating and taking into account the bulk density of the coating layer.

Batch experiment for pre-treatment unit

The adsorption process was tested by mixing 1 g/L from activated carbon and zeolite beads from the prepared activated carbon and zeolite

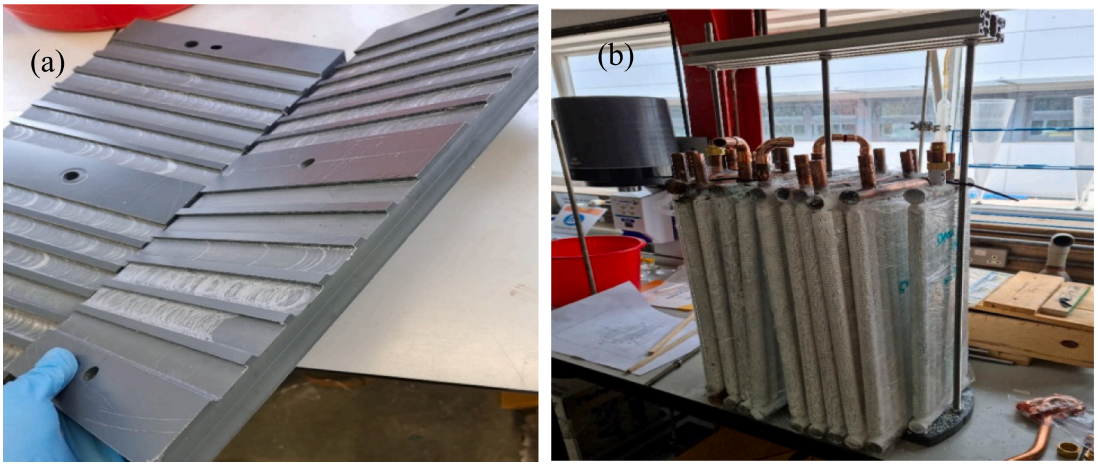

Fig. 7. (a) Plastic carrier of the heat exchanger and (b) Connecting the coated wire finned tube heat exchanger modules by soldering.

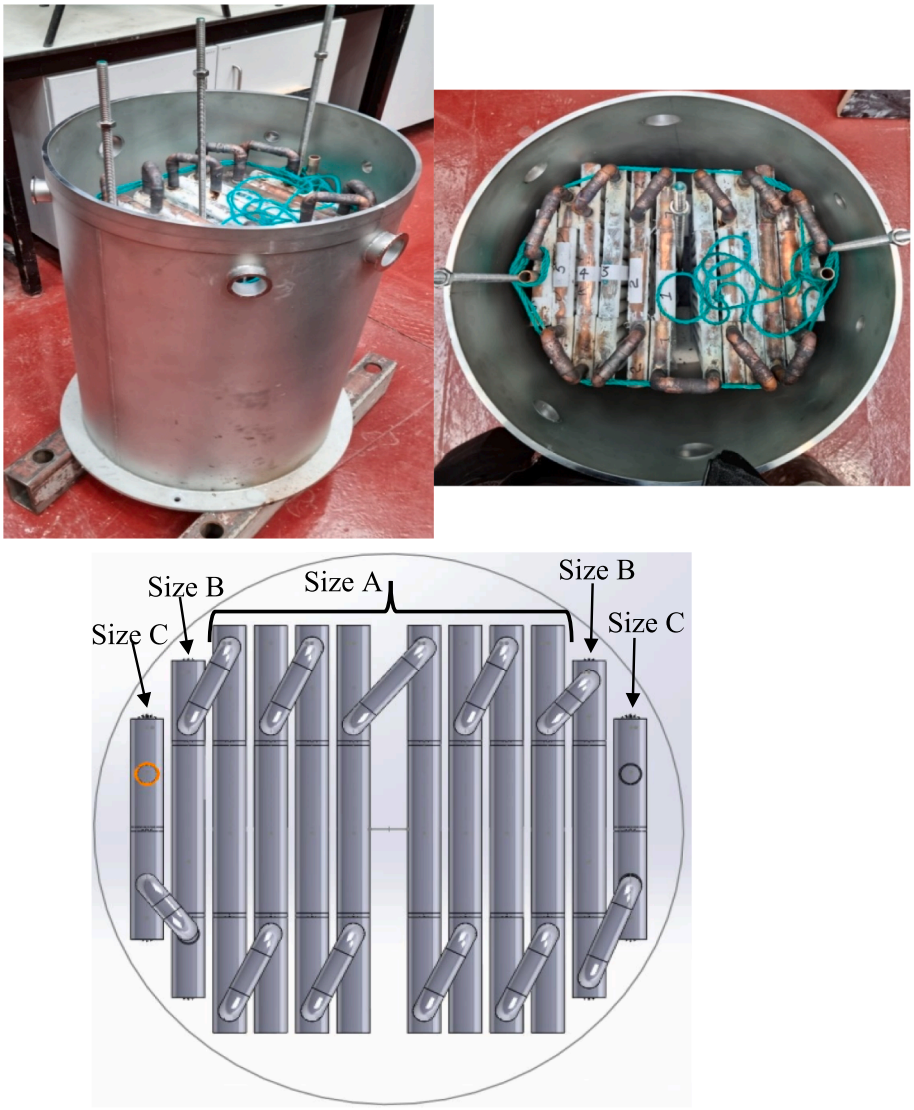

Fig. 8. Placing the heat exchanger modules inside the adsorber bed.

powder with 100 ml of synthetic wastewater polluted with heavy metals while stirring at 200 rpm at room temperature using batch technique to determine the materials selectivity as shown in Figure X3.

Assembly of the MOF adsorption heat pump for desalination and cooling unit

Fig. 6 illustrates the two-bed adsorption desalination and cooling system which consists of two adsorber beds, condenser and evaporator as the main components.

These components are connected using 50 mm copper pipe as vapour lines. These lines are controlled using four electrical solenoids ball valves to switch between the adsorption, desorption and switching processes. The two adsorber beds contain the aluminium fumarate MOF adsorbent material coated on the surface of wire finned heat exchanger modules. The adsorbent material is heated/cooled using another copper water line with a diameter of 28 mm. This line is also controlled using four three-way electrical solenoid ball valves. Thus, we have eight electrical valves that are controlled by LabView software using PC. This software is also used to input the preheating, switching and half cycle times as well as the number of the cycle used in testing. Three K type thermocouples (RS Pro 621–2158, with temperature range between −50 to 250 °C) are fitted in each chamber to measure the vapour and adsorbent material temperature, while RTD temperature sensors (RS Pro 123–5602, with temperature range between −50 to 250 °C) are used to measure the inlet and outlet water temperatures to the heat exchangers inside each chambers. The temperature readings of water, vapour and adsorbent material are stored using data logger (DT 85 series 4 Data-Taker). Feeding the water inside the system is controlled using temperature control led unit (ToolTemp – TT-138, 24 kW), adsorber bed water tank and pump for the adsorber beds, condenser water tank and pump for the condenser and another temperature control unit (ToolTemp – TT-188, 9 kW) and pump for the evaporator. A vacuum pump (nXDS dry scroll pump from Edwards Co) is connected to the various chambers through a manifold. Each adsorber bed has 12 heat exchanger modules coated with around 9 kg of adsorbent material. A rigid plastic carrier with 12 grooves are machined in order to fix the modules next to each other and ensure having a minimum gap of 3 mm between the modules as shown in Fig. 7. All the modules are connected in series by soldering the outlet of the module with the inlet of the next module using two copper elbows. The plastic carrier is connected with an aluminium bar profile using a steel threaded studs in order to be used for carrying the modules and place them inside the chamber.

Fig. 8 shows how the heat exchanger modules are placed inside the adsorber chamber with a diameter of 500 mm and height of 800 mm. The chamber dimensions are selected to minimize the dead volume

Table 1
Heat exchanger modules dimensions.

Parameters	value	Unit
Module size A		
Number of modules in each bed	8	
Module width	370	mm
Module length	600	mm
Number of tubes	14	
Header diameter	28	mm
Module size B		
Number of modules in each bed	2	
Module width	300	mm
Module length	600	mm
Number of tubes	12	–
Header diameter	28	mm
Module size C		
Number of modules in each bed	2	–
Module width	200	mm
Module length	600	mm
Number of tubes	8	–
Header diameter	28	mm
Tube geometry		
Tube diameter	10	mm
Fin height	7	mm
Fin spacing	2	mm
Number of fins	21	–
Fin thickness	0.7	mm

inside the cylinders.

Three module sizes are selected in order to be suitable with the cylindrical bed chamber to minimize the dead volume as shown in Table 1.

Figure X4 shows the heat exchanger copper coils fixed inside the evaporator and condenser chambers (internal diameter of 450 mm for each chamber). Each chamber has 60 m length of copper coil with a diameter of 3/8 in. The coils are connected in parallel by splitting the length of the coil into four portions, each one has 15 m' length. In the condenser, the coils are spread inside the chamber while they are kept flat inside the evaporator to minimize the water height that needs to cover the coils.

Testing procedure for the desalination and cooling unit

To prepare the adsorption system, the evaporator is filled with 8 to 12 L of water, then the lid is placed on the top of the evaporator chamber while any water inside the condenser chamber should be discharged through the bottom line underneath the condenser. Then, hot water is fed to the adsorber beds at temperature of 90 °C and flow rate between 20 L/min for an hour to ensure having fully dried adsorbent material before starting the experiment, followed by vacuuming all chambers by opening the valves in the manifold between the chambers and the vacuum pump. During or before the vacuuming process, the circulation water inside the condenser and evaporator are turned on. The vacuuming process is finished once the saturation pressure in the chambers reaches a value between 15 and 40 mbar based on the temperature of water flowing inside each chamber. Once the required pressure is achieved, all the vacuum valves in the vacuum manifold are closed as well as turning off the vacuum pump.

The operating temperatures, half cycle time, switching time and number of cycles are adjusted before starting the experiment using the LabView software. Then, the datalogger is initialized to store the temperature readings and the experiment is started. During the first 50 to 70 s, the hot water line that switched to a cold-water line, has an amount of hot water which will go to the cold-water tank and heat it up. Therefore, the cold-water tank temperature of the adsorber bed is controlled by switching on the drain line of the tank and starting feeding a tap water to the tank to compensate the increase in the water temperature of the tank. This step needs to be repeated every switching time. The same thing is happen in the temperature control unit since it has a hot water tank that has a temperature reduction possibility due to the cold water return during the switching time. Thus, all the temperatures and drain lines are controlled and monitored during the experiment to maintain a constant feeding temperature to the system. After finishing the experiment, all pumps and heaters are switched off, followed by extracting the temperature readings from the data logger.

Results and discussions

Contaminants removal performance of pre-treatment unit materials

Activated carbon

In order to test the metal ion adsorption selectivity of prepared nano-activated carbon beads from water hyacinth, its adsorption performance of was investigated against different polluted water samples containing one of the investigated heavy metals (lead, iron, manganese, and nickel). Where, 0.1 g of nano-activated carbon powder was mixed with 100 ml of synthetic polluted water at 50 ppm initial concentrations of each heavy metal separately under continuous stirring at 200 rpm at room temperature. After finishing the water treatment process, the adsorbent material was separated by centrifugation at different contact time interval (0–180 min) to determine the final pollutant concentration using atomic absorption spectroscopy. The pollutant removal percentage by synthesized nano-activated carbon was calculated by the following equation:

$$Removal\ \% = ((C_o - C_e)/C_o)*100$$

To track the removal efficiencies of each heavy metal separately, a sample of treated water was collected every 15 min and analysed by atomic absorption spectroscopy.

Figure X5(a) shows the removal results of each heavy metals separately. The results illustrated that the maximum removal achieved by nano-activated carbon material was recorded for the iron ions. On the other hand, the minimum decontamination percentage was recorded for nickel ions. Moreover, both manganese and nickel ions have approximately the same removal percentage with a slight difference after one hour. The equilibrium conditions were achieved after nearly 60 min of conducting the batch removal experiments for all studied metal ions. After testing heavy metals decontamination efficiencies onto nano-activated carbon individually, mixed heavy metals solution with a total pollutants concentration equal to 50 ppm were prepared, in other words, each metal ion concentration of lead, manganese, iron, and nickel has a concentration of 12.5 ppm with total pollutant concentration of 50 ppm. Every 15 min a water treated sample was withdrawn and analyzed by atomic absorption spectroscopy.

Figure X5(b) displays the removal percentages of the experiment conducted with water containing all metal contaminants. The results showed that the same adsorption behaviour for nano-activated carbon was followed by the mixed metal water solution. The maximum removal was recorded for iron ions, followed by lead and manganese, while the lowest separation efficiency was recorded for the nickel ions. The removal percentages of iron and lead were slightly close to each other. However, the adsorption percentages for manganese and nickel were close to each other with low removal values onto nano-activated carbon. The adsorption performances of the four different fabricated NAC/PES composite beads at the four different filler immobilization ratio (25, 45, 65 and 85 wt%) were compared against iron (12.5 ppm) metal separation as the nano-activated carbon achieved the maximum adsorption for iron metals compared with the remaining studied Ni, Mn and Pb metals. Batch adsorption was conducted through mixing 1 g/L from NAC/PES composite beads with synthetic water contaminated with iron metal, the stirring was kept at 200 rpm at room temperature for different time intervals. Every 15 min a water treated sample was withdrawn and

analysed by atomic absorption spectroscopy.

Figure X5(c) shows the results of the iron removal for the four different NAC/PES composite beads. It is clear that the only beads attain low iron removal with NAC immobilization ration of 25 % and the removal achieved by the remaining three NAC/PES 45 %, 65 % and 85 % beads have slightly little difference in the iron removal percentages. Therefore, the increment of NAC loading more than 45 % doesn't increase the iron decontamination percentages with a remarkable percent. So, NAC/PES composite beads with 45 % filler immobilization ratio were selected to be the optimum beads for further experiments.

The adsorption performance of the optimum fabricated NAC/PES 45 % composite beads was tested with the mixed metal ions contaminated solution with a total pollutant concentration equal to 50 ppm, in other words, each metal ion concentration at the synthetic wastewater stream of iron, lead, manganese, and nickel has a concentration of 12.5 ppm. Every 15 min a water treated sample was withdrawn and analysed by atomic absorption spectroscopy. Figure X5(d) shows the removal percentages of different metal contaminants using NAC/PES 45 % composite beads. The results showed that the maximum removal was recorded for iron metal, followed by lead, manganese and nickel. These results are showed similar behaviour for the previously tested free nano-activated carbon, confirming that the immobilization of nano-activated carbon onto PES polymer has no any effect on the adsorption performance of nano-activated carbon material.

Zeolite

Similar to the previous study of metal ion selectivity using nano-activated carbon and formulated NAC/PES beads, the prepared zeolite from the Egyptian clay is investigated. So, firstly the metal ions selectivity of zeolite powder material will be determined through preparation four of different wastewater streams containing different separated heavy metals of lead, iron, manganese, and nickel. Each heavy metal has a concentration of 50 ppm. The batch adsorption process was conducted by mixing 0.1 g from the prepared zeolite powder with 100 ml of synthetic wastewater polluted with every metal individually under stirring at 200 rpm and room temperature. To track the removal efficiencies of each heavy metal onto zeolite, a sample of treated water was collected every 15 min and analysed by atomic absorption spectroscopy.

Figure X7(a) shows the results of each heavy metals removal separately onto prepared zeolite. The result illustrates that the maximum removal achieved by the zeolite powder is for the lead ions and the minimum decontamination percentage is for the nickel removal.

Both manganese and iron metals have approximately the same removal percentage with a slight difference after an hour, but this difference is less than 5 %. So, these two metal ions may consider to have the same adsorption behavior onto the prepared zeolite. The equilibrium adsorption for the removal of various studied metal ions was achieved nearly between 1 and 1.5 h of conducting the batch removal experiments. After testing heavy metals decontamination efficiencies of zeolite individually, mixed heavy metals polluted solution with total pollutants concentration equal to 50 ppm was prepared with each metal (lead, manganese, iron, and nickel) has a concentration of 12.5 ppm. Every 15 min a water treated sample was withdrawn and analyzed by atomic absorption spectroscopy to monitor the adsorption behavior of zeolite toward the mixed metal polluted solution. Figure X6(b) displays the adsorption performance of zeolite toward different mixed metal ions. It was indicated that the same adsorption behavior was achieved by zeolite for the mixed solution, where the maximum removal was recorded for lead ions, followed by iron and manganese. However, the lowest adsorption was for the nickel ions. During the first hour, the removal percentages of the four heavy metals were close and ranged between 20 % and 30 %. After one hour, the difference in the removal percentages appeared and the increased to be between 35 % and 50 %. Similar to the previous study for nano-activated carbon/PES composite beads, the adsorption performances of the four different fabricated zeolite/PES composite beads at the four different filler immobilization ratio (25, 45, 65 and 85 wt%) were compared against lead (12.5 ppm) metal separation, the zeolite achieved the maximum adsorption for leads metals compared with the other studied metals. Batch adsorption was conducted through mixing 1 g/L from zeolite/PES composite beads with synthetic water contaminated with lead metal, the stirring was kept at 200 rpm at room temperature for different time intervals. Every 15 min a water treated sample was withdrawn and analyzed by atomic absorption spectroscopy. Figure X6(c) showed the results of the lead removal onto the four different prepared zeolite/PES composite beads. The data displays that the removal achieved by Zeolite/ PES 45 %, 65 % and 85 % beads have little difference in the lead removal percentages, that ranges between 40 % and 83 % over the studied time period. Therefore, loading the zeolite above 45 % did not produce significant increase in terms of the lead ions decontamination percentages. So, 45 % Zeolite/PES was selected to be the optimum fabricated beads to be used for the wastewater treatment further experiments. Therefore, the adsorption performance of 45 % zeolite/PES composite beads against mixed contaminated metal ions solution will be investigated. Mixed heavy metals solution with a total pollutants concentration equals to 50 ppm was prepared, in other words each metal of lead, manganese, iron and nickel has a concentration of 12.5 ppm at the mixed metals solution. Each 15 min a water treated sample was withdrawn and analyzed by atomic absorption spectroscope. Figure X6(d) showed the removal percentages of different metal ions contaminants using 45 % zeolite/PES composite beads. The results showed that the maximum removal was recorded for lead, followed by iron, manganese and nickel similar to adsorption behavior of zeolite powder.

Table 2
Operating conditions.

Parameters	value	Unit
Adsorption water flowrate (in each chamber)	25	L/min
Desorption water flowrate (in each chamber)	20	L/min
Chilled water flowrate	25	L/min
Condenser water flowrate	30	L/min
Inlet water adsorption temperature	25,30,35,40 and 45	°C
Inlet heating temperature	90,80,70, 60 and 50	°C
Inlet chilled water temperature	13, 18, 23, 27 and 31	°C
Inlet condenser water temperature	25	°C
Switching time	70	*sec*

Expected pure water production from pre-treatment unit

Since the desalination and cooling unit will produce more than 260 L/day, the feeding purified water to the evaporator should be higher than the water production by taking into account submerging the coils of the evaporator during the operation by at least 10*L*. Additionally, assuming that 30 % of the water will not be evaporated and will be discharged as a brine water. Thus, the pre-treatment unit should have a purified water capacity production of 350 L/day. Activated carbon or zeolite/PES 45 % composite beads are the selected material for the pre-treatment unit for water that contains of 50 ppm Fe, Pb, Mn and Ni. Figure X7(a) shows that the activated carbon gives the maximum absorption capacity of 87 % for Fe, while zeolite has 77 % absorption capacity for this metal. This metal removal experiment was conducted using 100 ml of water with 1 g of adsorbent material for three and two hours using activated carbon and zeolite respectively. The rinsing process to reuse the material for the next cycle takes around an hour by soaking the material in fresh water. Therefore, the cycle time for the activated carbon and zeolite is four and three hours respectively. This indicates that the specific purified water daily productions of the material are 6 and 8 m3/kg/day for activated carbon and zeolite respectively as shown in Figure X7(b). Thus, to produce 350L/day of purified water that can be used in the evaporator of the desalination and cooling unit, 58.3 g of activated carbon or 43.75 g of zeolite is required.

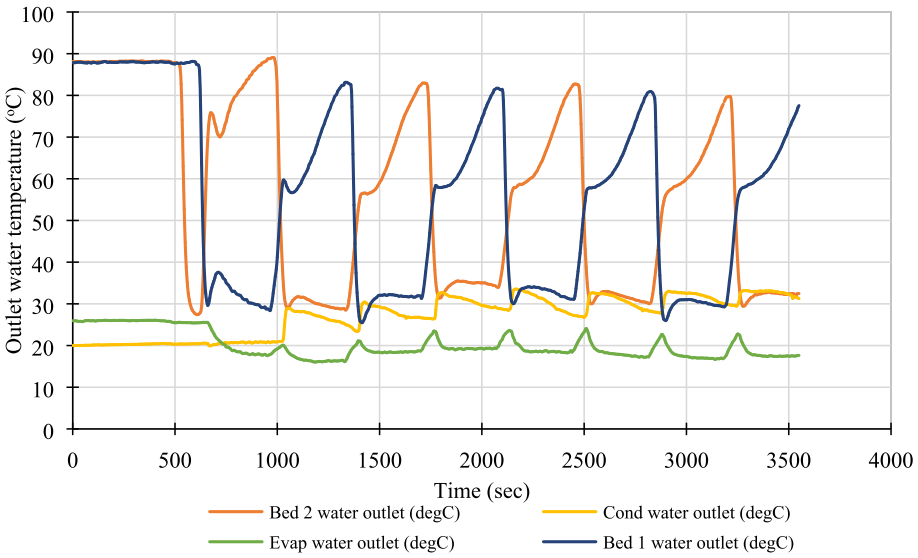

Fig. 9. Temperature variation with time ($T_{cooling}$ = 25 °C, $T_{heating}$ = 90 °C, $T_{chilled}$ = 23 °C and $t_{halfcycle}$ = 200 *sec*).

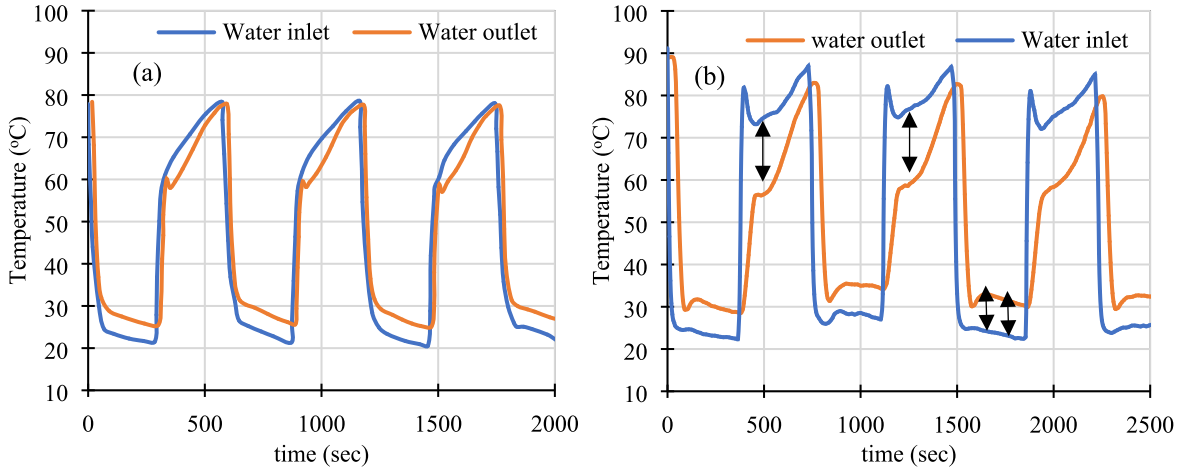

Fig. 10. Temperature profile of inlet/outlet to/from the adsorber bed (a) packed heat exchanger and (b) coated heat exchanger.

Desalination and cooling unit performance

The operating conditions used in the experiment are illustrated in Table 2. At an inlet heating temperature of 90 °C, cooling temperature of 25 °C, chilled water temperature of 23 °C and half cycle time of 200 s, the desalination and cooling unit is set to be the reference case in the study.

Fig. 9 shows the water outlet temperature profile in each component in the adsorption system for four cycles. The system was started by drying the adsorbent material in the two beds to ensure having fully dried material before starting the system. An average outlet chilled water temperature of 18 °C is maintained during all cycles with an increase of 4°is observed during the switching time in which a significant reduction in cooling energy is detected during this interval (70 s). The switching time is adjusted to suit the energy required to heat up the heat exchangers (12 modules connected in series). Additionally, once the valve between the evaporator and adsorber bed is switched on, a significant amount of water vapor is passed to the bed which causes a temperature increase in the bed due to the large amount of water vapor that suddenly enter the bed which is adsorbed releasing amount of adsorption heat.

The inlet water temperature was tried to be constant during the experiment, however there was a variation in the inlet heating temperature between 88 and 75 °C due to the limited water storage capacity. Fig. 10 illustrates the difference between the inlet and outlet water temperatures in the adsorber bed using the packed heat exchanger from Albaik et al. [34] experiment and coated heat exchanger in this study. It is observed from the temperature differences that the energy consumption in the regeneration process using the coated method is higher than the packed one in order to produce the same amount of distilled water and cooling power, while the required coated adsorbent material is less than the required one using the packed method. It is important to illustrate that a sudden increase or decrease in the outlet water temperature is observed as an indication of ending the switching process between the adsorption and desorption processes so that the valve between the adsorber bed and the condenser/evaporator is opened to allow the water vapor to be transferred from/to the adsorber bed. This causes a significant change in the vapor content inside the adsorber bed. A significant amount of heat is also generated/absorbed due to the heat of adsorption at this period.

Effect of half cycle time and operating temperatures

The performance of the system is analysed based on daily water production (DWP), specific daily water production (SDWP), cooling power (CP), and coefficient of performance (COP), which are calculated as follows:

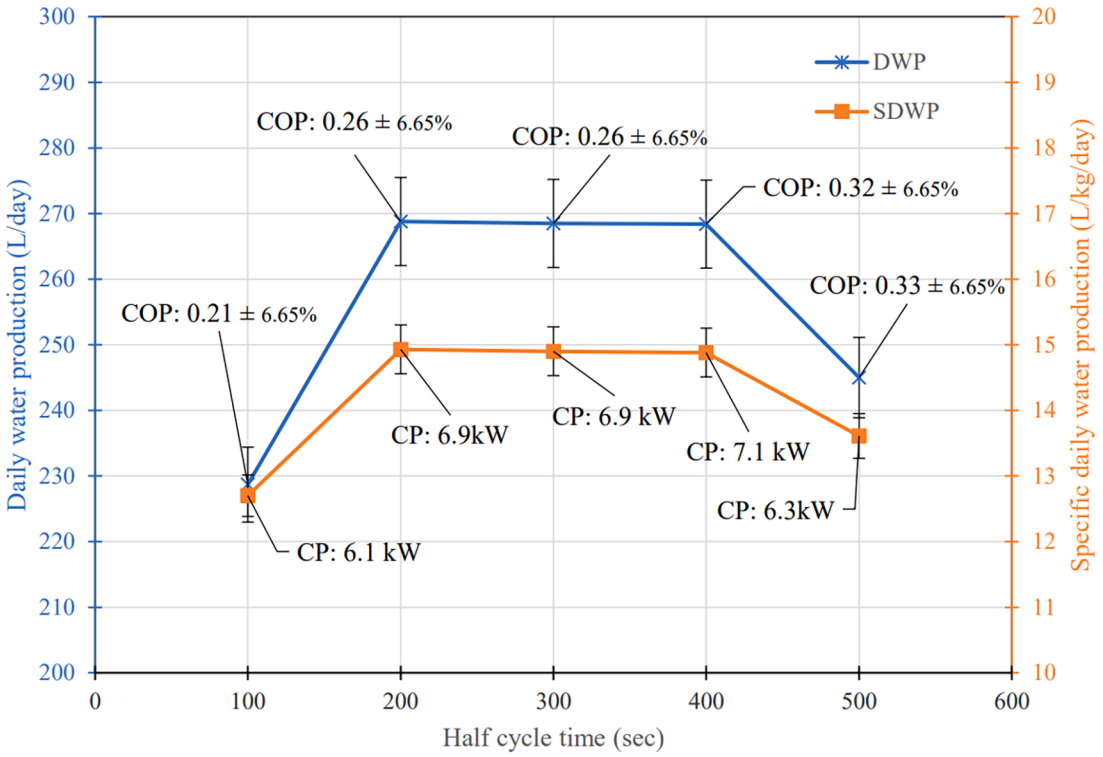

Fig. 11. Effect of half cycle time on daily water production and specific daily water production. (T_{des} = 90 °C, $T_{chilled}$ = 23 °C, T_{cond} = 25 °C, T_{ads} = 25 °C).

$$DWP = \frac{L_{water}}{t_{cycle}}\left(t_{day}\right) \quad (1)$$

$$SDWP = \frac{DWP}{M_{ads}} \quad (2)$$

$$CP = \frac{Q_{evap}}{t_{cycle}} \quad (3)$$

$$Q_{evap} = \frac{\sum_{t_{ads}+t_{sw}}[\dot{m}_{chilled}C_p(T_{ch,in} - T_{ch,out})\Delta t]}{t_{ads} + t_{sw}} \quad (4)$$

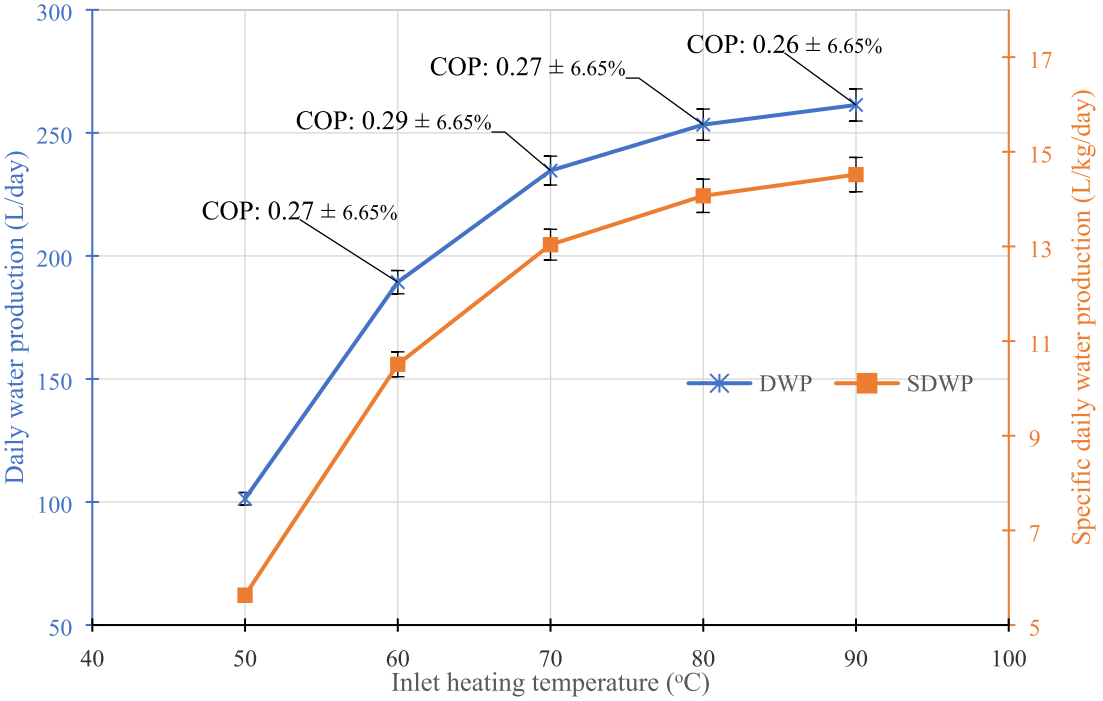

Fig. 12. Effect of inlet heating temperature (desorption temperature) on daily water production and specific daily water production ($t_{half\ cycle}$ = 200 *sec*, $T_{chilled}$ = 23 °C, T_{cond} = 25 °C, T_{ads} = 25 °C).

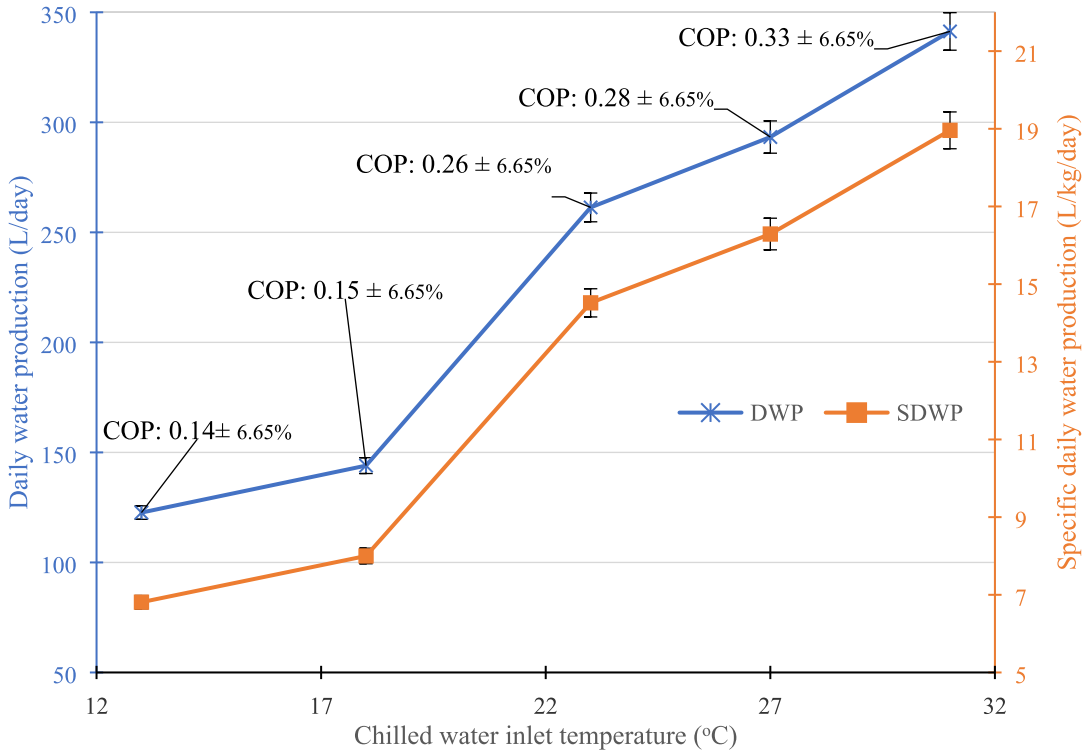

Fig. 13. Effect of chilled water inlet temperature (in evaporator) on daily water production and specific daily water production ($t_{half\ cycle}$ = 200 *sec*, T_{des} = 90 °C, T_{cond} = 25 °C, T_{ads} = 25 °C).

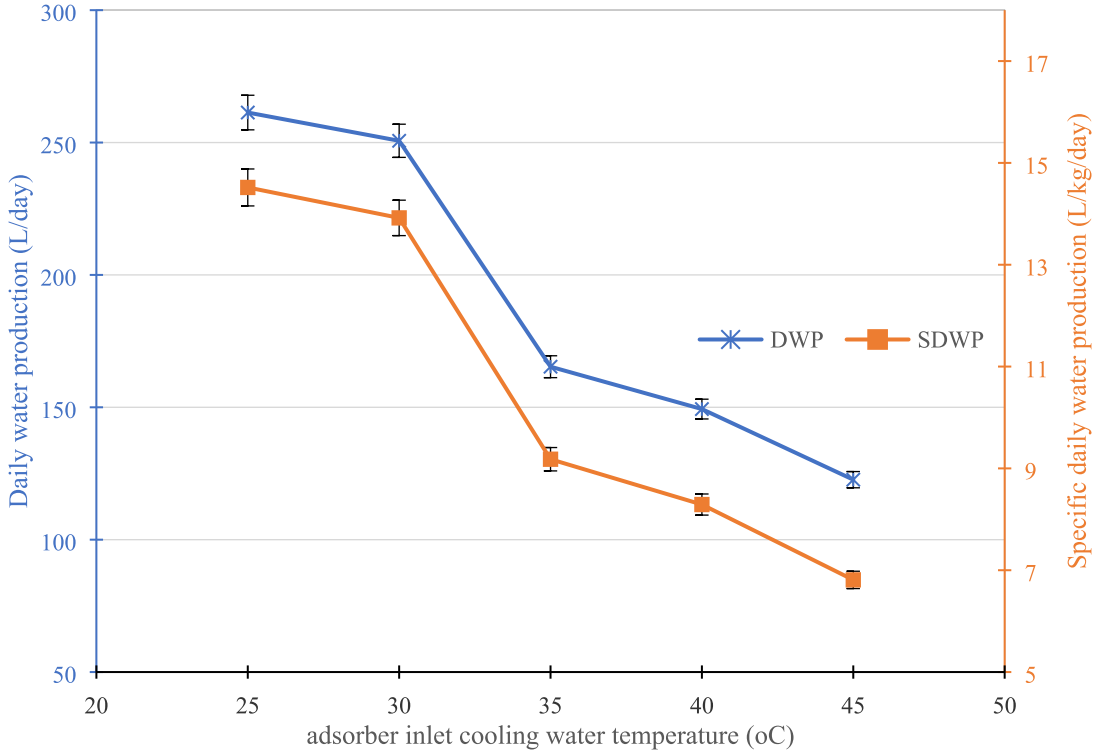

Fig. 14. Effect of adsorber inlet cooling water temperature on daily water production and specific daily water production ($t_{half\ cycle}$ = 200 *sec*, T_{des} = 90 °C, T_{cond} = 25 °C, $T_{chilled}$ = 23 °C).

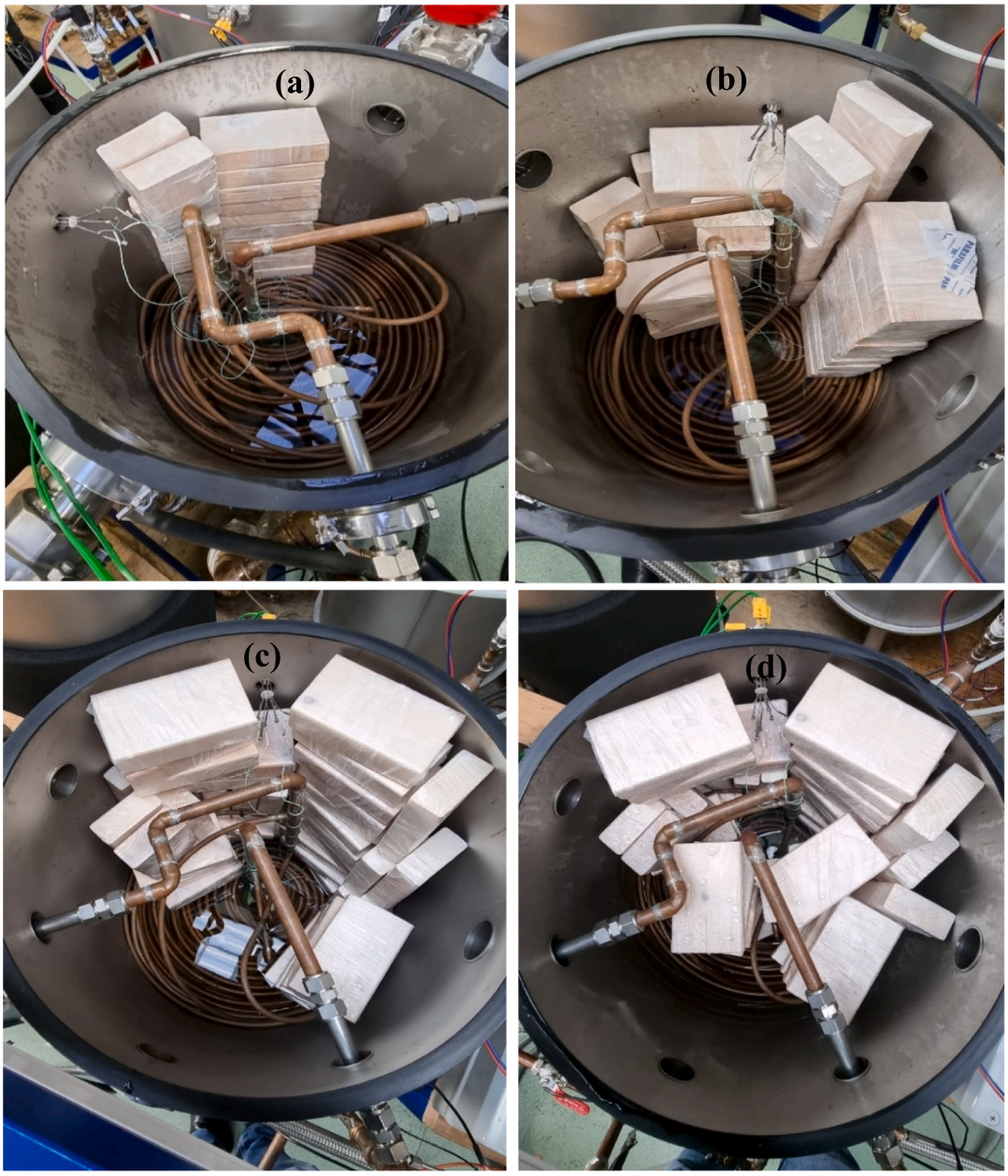

Fig. 15. Evaporator chamber (a) 12.5% occupied, (b) 25% occupied, (c) 37.5% occupied and (d) 50% occupied.

$$COP = \frac{Q_{evap}}{Q_{des}} \tag{5}$$

$$Q_{des} = \frac{\sum_{t_{des}+t_{sw}} [\dot{m}_{des} C_p (T_{des,in} - T_{des,out}) \Delta t]}{t_{des} + t_{sw}} \tag{6}$$

Where L_{water} is the collected water from the condenser, t_{cycle} is the cycle time, t_{sw} is the switching time M_{ads} is the adsorbent material mass, Q_{evap} is the cooling rate in the evaporator, Q_{des} is the heating energy, $\dot{m}_{des}$ is the mass flow rate of heating water, $\dot{m}_{chilled}$ is the mass flow rate of the chilled water and Δt is the time step in the data logger.

Before carrying on a parametric study to investigate the effect of various operating temperatures on the performance of the adsorption system, the optimum half cycle time is investigated and the result are shown in Fig. 11. It is observed that the optimum half cycle time is between 200 and 300 s where the maximum daily water production (DWP) and cooling power are around 268 L/day and 6.9 kW respectively, while the specific daily water production (SDWP) is 14.9 L/kg/day. A significant drop in water production is observed when the half cycle time is lower than 200 s and higher than 400 s. The short half cycle time indicates that the kinetics of the adsorbent material is significantly improved due to the coating technique which eliminates the thermal contact resistance and increases the effective thermal conductivity. The COP of the system is also studied at different half cycle times which showed that increasing the half cycle time will enhances the COP from 0.21 at half cycle time of 100 s and reached to 0.33 at half cycle time of 500 s. This can be justified due to the heating energy needed to heat up the adsorbent material is significantly decreased while the cooling production showed slight reduction. This is due to the significant amount of energy that required at the beginning of the cycle to heat up 12 heat exchanger modules before heating the adsorbent material itself. After a period of time, this energy is only used to regenerate the material while almost no energy will be required for the metal masses.

Fig. 12 shows the effect of inlet heating temperature on the adsorption system performance. The results showed that the system is still effective as long as the heating temperature does not drop below

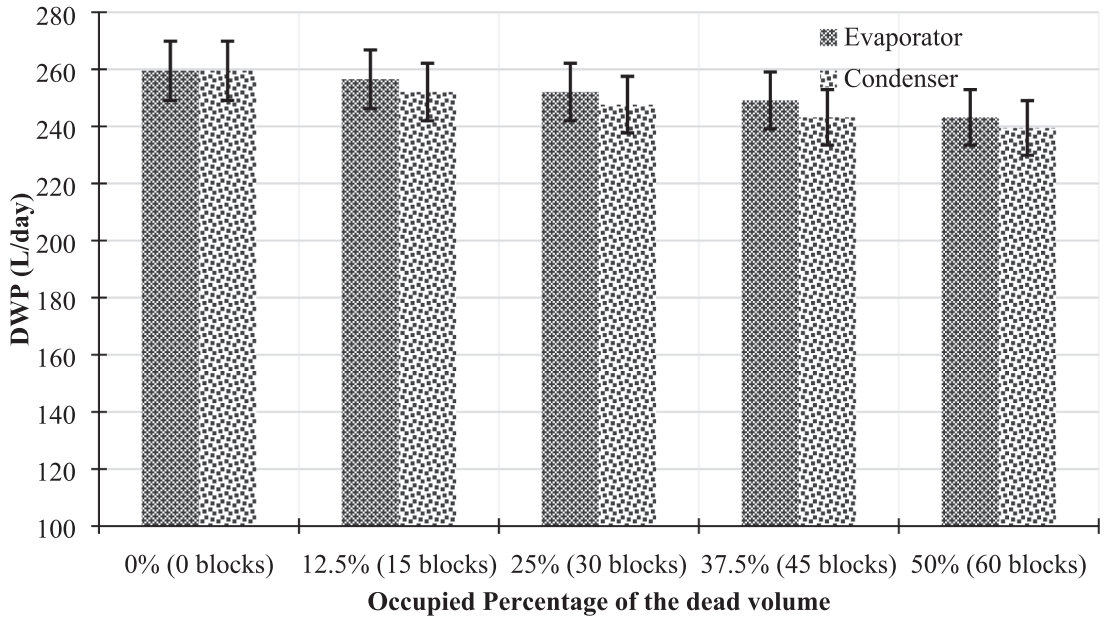

Fig. 16. Effect of the dead volume in the evaporator and condenser chambers on the water production.

70 °C. This shows the advantage of the aluminium fumarate adsorbent material as it requires a relatively low heating temperature in order to desorb the water vapour. Aluminium fumarate has a high reversable water adsorption with the isotherm of S shape, which is reflected by the moderate isosteric heat of adsorption. The maximum COP of the system was found at heating temperature of 70 °C and any increase in the heating temperature will cause a reduction in the COP, which indicates that the heating energy at this temperature is sufficient to produce the same amount of water production/cooling power at higher heating temperature.

Fig. 13 shows the effect of the chilled water inlet temperature to the evaporator on the system performance. The results showed that this temperature has a significant impact on the system performance since the water production is dramatically increased when the temperature equal or higher than 23 °C. On the other hand, at low chilled inlet water temperature, the system is no longer effective as the performance dropped more than 50 %. The effect of this temperature on the system performance can be explained using the adsorption isotherm of the aluminium fumarate which has S shape relation between the relative pressure and water uptake in which at a low relative pressure (lower than 0.2), the equilibrium uptake is very low. While a significant increase in the water uptake is observed at relative pressure between 0.2 and 0.3. Therefore, this adsorption system using aluminium fumarate is very effective at higher evaporation temperature, which also can be indicated from the COP values.

Fig. 14 investigates the effect of the adsorption inlet water temperature giving the same impact as the chilled water temperature on the system performance. It is observed that the adsorber bed should have a cooling temperature of 30 °C or lower to maintain the system performance.

Evaporator and condenser dead volume effects

One of the critical factors that has been overlooked in the literature, is the design of the evaporator and condenser in the adsorption system in terms of the available void volume above the heat exchanger. Many studies investigated the coil performance in terms of the overall heat transfer coefficient by introducing different tube design such as plain and coated tubes as well as capillary-assisted tubes [35]. While the volume of the chambers of the condenser and evaporator that represents about half of the adsorption system volume need to be optimized and reduced. Therefore, an investigation on the effect of dead volume in the condenser and evaporator was carried out by occupying the dead volume with insulated wooden blocks (40 mm × 90 mm × 150 mm). The wood material is selected to minimize the thermal mass impact on the heat transfer coefficient as well as the very low thermal conductivity of this material. A number of blocks are placed in the condenser and evaporator to occupy 12.5, 25, 37.5 and 50 % of the dead volume as shown in Fig. 15.

By taking into account the uncertainty in the results, it was found that by occupying 50 % of the dead volume or less, the daily water production remained almost constant as shown in Fig. 16. The slight reduction in the daily water production is due to the obstruction of the vapor flow from the evaporator to the adsorber bed or from the adsorber bed to the condenser caused by the wooden blocks which lower the water production at any given cycle time. This indicates that 50 % of the dead volume in the chamber can be removed. The internal diameter of the chamber is 450 mm while the height of the dead volume in the evaporator chamber is 400 mm. Thus, the chamber height can be reduced by 200 mm, so the overall height of the chamber will be 400 mm (200 mm the height of the water that fully submerge the coils plus 200 mm dead volume).

Conclusions

In this work, a hybrid system consists of a pre-treatment unit and a desalination and cooling unit has been studied using different adsorbent materials. Activated carbon and zeolite has been tested in the forms of powder and beads for the removal of different heavy metals from ground water and it was found that the optimum loading of PES is 45 % for the bead's formation. Activated carbon showed the highest removal for Iron (87 %), while zeolite has the highest removal for lead (75 %). More importantly, these results showed that activated carbon and zeolite can be applied as a purifying material in the pre-treatment unit and feed stock to the desalination and cooling unit with a specific purified water daily production of 6 and 8 m^3/kg/day using activated carbon and zeolite respectively.

Aluminium fumarate MOF material with different coating thicknesses was characterised and identified as potential Metal Organic framework materials for desalination and cooling unit after receiving the purified water to the evaporator of the unit. A coating process was successfully developed for integrating the aluminium fumarate MOF material to the heat exchanger metal surfaces used in the adsorber beds.

This coating process was shown to improve the adsorption system performance through reducing the thermal resistance between the heating and cooling fluids and the adsorbent material during desorption and adsorption. The desalination and cooling unit has a production of more than 260 L/day of distilled water and 6.9 kW of cooling. The hybrid system has a potential to be more compact after conducting an experiment on the effect of dead volume in the evaporator and condenser chambers on the system production and it was found that these component volumes can be significantly decreased where 50 % of their dead volume can be removed.

CRediT authorship contribution statement

Ibrahim Albaik: Conceptualization, Methodology, Data curation, Writing – original draft, Visualization, Investigation, Writing – review & editing. **Kamal Diab:** Conceptualization, Methodology, Data curation, Writing – original draft, Visualization, Investigation, Writing – review & editing. **Majdi Saleh:** Participating in building the desalination system. **Raya Al-Dadah:** Supervision, Validation, Writing – review & editing, Project administration, Resources. **Saad Mahmoud:** Supervision, Project administration. **Mahmoud B. Elsheniti:** Methodology, Data curation, Writing – review & editing. **İsmail Solmaz:** Methodology, Data curation, Writing – review & editing. **Eslam Salama:** Visualization, Investigation. **H. Shokry Hassan:** Visualization, Investigation. **Marwa F. Elkadi:** Supervision, Project administration.

Declaration of Competing Interest

The authors declare that they have no known competing financial interests or personal relationships that could have appeared to influence the work reported in this paper.

Data availability

No data was used for the research described in the article.

Acknowledgement

The authors would like to thank the British Council Institutional Links grant, “NewtonMusharafa” and their partner “Science and Technology Development Fund (STDF), Egypt” for sponsoring this project with the grant number 332436905.

Appendix:. Uncertainty calculations of cooling power, specific water daily production, daily water production and coefficient of performance.

To estimate the uncertainty in calculating the CP, SDWP, DWP and COP of the adsorption system, the following equations are used:

$$\frac{U_{CP}}{CP}=\sqrt{\left(\frac{U_{Cp}}{Cp}\right)^2+\left(\frac{U_{\dot{m}_{chilled}}}{\dot{m}_{chilled}}\right)^2+\left(\frac{U_{T_{chilled,in}}}{T_{chilled,in}-T_{chilled,out}}\right)^2+\left(\frac{U_{T_{chilled,out}}}{T_{chilled,in}-T_{chilled,out}}\right)^2} \tag{7}$$

$$\frac{U_{SDWP}}{SDWP}=\sqrt{\left(\frac{U_{collectedwateramount}}{collectedwateramount}\right)^2+\left(\frac{U_{adsmass}}{adsmass}\right)^2} \tag{8}$$

$$\frac{U_{DWP}}{DWP}=\sqrt{\left(\frac{U_{collectedwateramount}}{collectedwateramount}\right)^2} \tag{9}$$

$$\frac{U_{COP}}{COP}=\sqrt{\left(\frac{U_{Cp}}{Cp}\right)^2+\left(\frac{U_{\dot{m}_{chilled}}}{\dot{m}_{chilled}}\right)^2+\left(\frac{U_{\dot{m}_{des}}}{\dot{m}_{des}}\right)^2+\left(\frac{U_{T_{chilled,in}}}{T_{chilled,in}-T_{chilled,out}}\right)^2+\left(\frac{U_{T_{chilled,out}}}{T_{chilled,in}-T_{chilled,out}}\right)^2+\left(\frac{U_{T_{des,in}}}{T_{des,in}-T_{des,out}}\right)^2+\left(\frac{U_{T_{des,out}}}{T_{des,in}-T_{des,out}}\right)^2} \tag{10}$$

Where

U_{SCP}	Is the uncertainty of the calculated SCP
U_{CP}	Is the uncertainty of the calculated CP
U_{SDWP}	Is the uncertainty of the calculated SDWP
U_{DWP}	Is the uncertainty of the calculated DWP
U_{COP}	Is the uncertainty of the calculated COP
U_{Cp}	Is the uncertainty in the specific heat of the water which assumed to be zero as the value is extracted from tabulated property data
$U_{\dot{m}_{chilled}}$	Is the uncertainty in reading the flow rate of the chilled water in the evaporator. The flow meter has uncertainty of 0.25 L/min
$U_{\dot{m}_{des}}$	Is the uncertainty in reading the flow rate of the desorption water in the adsorber bed. The flow meter has uncertainty of 0.25 L/min
$U_{T_{chilled,in}}$	Is the uncertainty in reading the inlet chilled water temperature in the evaporator. It is measured using the RTD thermocouple with uncertainty of 0.179 °C
$U_{T_{chilled,out}}$	Is the uncertainty in reading the outlet chilled water temperature in the evaporator. It is measured using the RTD thermocouple with uncertainty of 0.179 °C
$U_{T_{des,in}}$	Is the uncertainty in reading the inlet desorption water temperature in the adsorber bed. It is measured using the RTD thermocouple with uncertainty of 0.179 °C
$U_{T_{des,out}}$	Is the uncertainty in reading the outlet desorption water temperature in the adsorber bed. It is measured using the RTD thermocouple with uncertainty of 0.179 °C
$U_{adsmass}$	Is the uncertainty in measuring the mass of the adsorbent. The mass of adsorbent is measured using digital balance with uncertainty of 0.005 kg
$U_{collectedwateramount}$	Is the uncertainty in the reading of the measuring cylinder which has uncertainty of 25 ml.

Thus, the maximum uncertainties for SCP, CP, SDWP, DWP and COP are 4.705, 4.703, 2.503, 2.501 and 6.654 % respectively.

Appendix A. Supplementary data

Supplementary data to this article can be found online at https://doi.org/10.1016/j.seta.2022.103006.

References

[1] WWAP. "The United Nations World Water Development Report 4: Managing Water Under Uncertainty and Risk, UNESCO". 2012.

[2] Schwarzenbach RP, Egli T, Hofstetter TB, von Gunten U, Wehrli B. Global water pollution and human health. Annu Rev Env Resour 2010;35(1):109–36. https://doi.org/10.1146/annurev-environ-100809-125342.

[3] WHO. "Guidelines for Drinking-Water Quality, WHO". 2017.

[4] Kosikowska M, Biziuk M. Review of the determination of pesticide residues in ambient air. TrAC Trends Anal Chem 2010;29(9):1064–72. https://doi.org/10.1016/j.trac.2010.06.008.

[5] Amooey AA, Ghasemi S, Mirsoleimani-azizi SM, Gholaminezhad Z, Chaichi MJ. Removal of Diazinon from aqueous solution by electrocoagulation process using aluminum electrodes. Korean J Chem Eng 2014;31(6):1016–20. https://doi.org/10.1007/s11814-014-0032-4.

[6] Wang C, Shih Y. Degradation and detoxification of diazinon by sono-Fenton and sono-Fenton-like processes. Sep Purif Technol 2015;140:6–12. https://doi.org/10.1016/j.seppur.2014.11.005.

[7] Mirsoleimani-azizi SM, Setoodeh P, Samimi F, Shadmehr J, Hamedi N, Rahimpour MR. Diazinon removal from aqueous media by mesoporous MIL-101 (Cr) in a continuous fixed-bed system. J Environ Chem Eng 2018;6(4):4653–64. https://doi.org/10.1016/j.jece.2018.06.067.

[8] Reigart JR, Roberts JR. "Organophosphate insecticides".

[9] Matouq MA, Al-Anber ZA, Tagawa T, Aljbour S, Al-Shannag M. Degradation of dissolved diazinon pesticide in water using the high frequency of ultrasound wave. Ultrason Sonochem 2008;15(5):869–74. https://doi.org/10.1016/j.ultsonch.2007.10.012.

[10] Mirsoleimani-azizi SM, Amooey AA, Ghasemi S, Salkhordeh-panbechouleh S. Modeling the removal of endosulfan from aqueous solution by electrocoagulation process using artificial neural network (ANN). Ind Eng Chem Res 2015;54(40):9844–9. https://doi.org/10.1021/acs.iecr.5b02846.

[11] Sarkar B, Venkateswralu N, Rao RN, Bhattacharjee C, Kale V. Treatment of pesticide contaminated surface water for production of potable water by a coagulation-adsorption-nanofiltration approach. Desalination 2007;212(1–3):129–40. https://doi.org/10.1016/j.desal.2006.09.021.

[12] TANWEER AHMAD, MOHD RAFATULLAH, ARNIZA GHAZALI, OTHMAN SULAIMAN, and ROKIAH HASHIM, "Removal of Pesticides from Water and Wastewater by Different Adsorbents: A Review".

[13] Zhao Z, Li X, Li Z. Adsorption equilibrium and kinetics of p-xylene on chromium-based metal organic framework MIL-101. Chem Eng J 2011;173(1):150–7. https://doi.org/10.1016/j.cej.2011.07.051.

[14] Marzbali MH, Esmaieli M, Abolghasemi H, Marzbali MH. Tetracycline adsorption by H3PO4-activated carbon produced from apricot nut shells: a batch study. Process Saf Environ Prot 2016;102:700–9. https://doi.org/10.1016/j.psep.2016.05.025.

[15] Marzbali MH, Mir AA, Pazoki M, Pourjamshidian R, Tabeshnia M. Removal of direct yellow 12 from aqueous solution by adsorption onto spirulina algae as a high-efficiency adsorbent. J Environ Chem Eng 2017;5(2):1946–56. https://doi.org/10.1016/j.jece.2017.03.018.

[16] Gupta VK, Saleh TA. Sorption of pollutants by porous carbon, carbon nanotubes and fullerene- An overview. Environ Sci Pollut Res 2013;20(5):2828–43. https://doi.org/10.1007/s11356-013-1524-1.

[17] Shahzad MW, Burhan M, Ang L, Ng KC. "Adsorption desalination-Principles, process design, and its hybrids for future sustainable desalination," in *Emerging Technologies for Sustainable Desalination Handbook*, Elsevier, 2018, pp. 3–34. doi: 10.1016/B978-0-12-815818-0.00001-1.

[18] Mezher T, Fath H, Abbas Z, Khaled A. Techno-economic assessment and environmental impacts of desalination technologies. Desalination 2011;266(1–3):263–73. https://doi.org/10.1016/j.desal.2010.08.035.

[19] Lenzen D, Zhao J, Ernst SJ, Wahiduzzaman M, Ken Inge A, Fröhlich D, et al. A metal–organic framework for efficient water-based ultra-low-temperature-driven cooling. Nat Commun 2019;10:1–9. https://doi.org/10.1038/s41467-019-10960-0.

[20] Elsayed E, AL-Dadah R, Mahmoud S, Anderson PA, Elsayed A, Youssef PG. CPO-27 (Ni), aluminium fumarate and MIL-101(Cr) MOF materials for adsorption water desalination. Desalination 2017;406:25–36.

[21] Saleh MM, Elsayed E, AL-Dadah R, Mahmoud S. Experimental testing of wire finned heat exchanger coated with aluminium fumarate MOF material for adsorption desalination application. Therm Sci Eng Progress 2022;28:101050. https://doi.org/10.1016/j.tsep.2021.101050.

[22] Lee SJ, Lim HW, Park SH. Adsorptive seawater desalination using MOF-incorporated Cu-alginate/PVA beads: Ion removal efficiency and durability. Chemosphere 2021;268:128797. https://doi.org/10.1016/j.chemosphere.2020.128797.

[23] Lee H, Ahn C, Khalfaoui W, Mishra B, Lee E, Jo I. Effects of iron oxidation state and chromium distribution on the corrosion resistance of high interstitial stainless steel for down-hole application. Metals (Basel) Oct. 2020;10(10):1–8. https://doi.org/10.3390/met10101302.

[24] Xu J, Wang L, Zhu Y. Decontamination of Bisphenol A from aqueous solution by graphene adsorption. Langmuir 2012;28(22):8418–25. https://doi.org/10.1021/la301476p.

[25] Mohan D, Pittman CU. Arsenic removal from water/wastewater using adsorbents—A critical review. J Hazard Mater 2007;142(1–2):1–53. https://doi.org/10.1016/j.jhazmat.2007.01.006.

[26] Ren J, Musyoka NM, Langmi HW, Swartbooi A, North BC, Mathe M. A more efficient way to shape metal-organic framework (MOF) powder materials for hydrogen storage applications. Int J Hydrogen Energy 2015;40(13):4617–22. https://doi.org/10.1016/j.ijhydene.2015.02.011.

[27] Valizadeh B, Nguyen TN, Smit B, Stylianou KC. Porous metal-organic Framework@Polymer beads for iodine capture and recovery using a gas-sparged column. Adv Funct Mater 2018;28(30):1801596. https://doi.org/10.1002/adfm.201801596.

[28] Rezk A, Al-Dadah RK, Mahmoud S, Elsayed A. Effects of contact resistance and metal additives in finned-tube adsorbent beds on the performance of silica gel/water adsorption chiller. Appl Therm Eng May 2013;53(2):278–84. https://doi.org/10.1016/j.applthermaleng.2012.04.008.

[29] Caprì A, Frazzica A, Calabrese L. Recent developments in coating technologies for adsorption heat pumps: a review. Coatings 2020;10(9):855.

[30] Tatlier M. Theoretical investigation of performances of zeolite Y and SAPO-34 coatings for adsorption heat pump applications. Heat and Mass Transfer/Waerme- und Stoffuebertragung 2021;57(6):975–84. https://doi.org/10.1007/s00231-020-03003-8.

[31] Yang S, Peng L, Syzgantseva OA, Trukhina O, Kochetygov I, Justin A, et al. Preparation of highly porous metal-organic framework beads for metal extraction from liquid streams. J Am Chem Soc 2020;142(31):13415–25.

[32] Albaik I, Al-Dadah R, Mahmoud S, Ismail MA, Almesfer MK. Coated, packed and combined wire finned tube adsorption cooling and desalination system using metal-organic framework: numerical study. Energy 2022;247:123506. https://doi.org/10.1016/j.energy.2022.123506.

[33] Elsayed E, Saleh MM, AL-Dadah R, Mahmoud S, Elsayed A. Aluminium fumarate metal-organic framework coating for adsorption cooling application: experimental study. Int J Refrig 2021;130:288–304. https://doi.org/10.1016/j.ijrefrig.2021.05.015.

[34] Albaik I, Badawy Elsheniti M, Al-Dadah R, Mahmoud S, Solmaz İ. Numerical and experimental investigation of multiple heat exchanger modules in cooling and desalination adsorption system using metal organic framework. Energy Convers Manag 2022;251:114934. https://doi.org/10.1016/j.enconman.2021.114934.

[35] Lanzerath F, Seiler J, Erdogan M, Schreiber H, Steinhilber M, Bardow A. The impact of filling level resolved: capillary-assisted evaporation of water for adsorption heat pumps. Appl Therm Eng 2016;102:513–9. https://doi.org/10.1016/j.applthermaleng.2016.03.052.